Chemical Science

ROYAL SOCIETY OF CHEMISTRY

EDGE ARTICLE

View Article Online
View Journal | View Issue

Cite this: *Chem. Sci.*, 2023, **14**, 13799

All publication charges for this article have been paid for by the Royal Society of Chemistry

Received 10th August 2023
Accepted 6th November 2023

DOI: 10.1039/d3sc04183b

rsc.li/chemical-science

A series of caged fluorophores for calibrating light intensity†

Mrinal Mandal, [a] Hessam Sepasi Tehrani,[a] Qianhua Mai,[a] Emma Simon,[a] Marie-Aude Plamont, [a] Christine Rampon,[b] Sophie Vriz,[b] Isabelle Aujard,*[a] Thomas Le Saux *[a] and Ludovic Jullien *[a]

Absolute measurement of light intensity is sought for in multiple areas of chemistry, biology, physics, and engineering. It can be achieved by using an actinometer from analyzing the time-course of its reaction extent on applying constant light. However, most reported actinometers exploit the absorbance observable for reporting the reaction extent, which is not very sensitive nor relevant in imaging systems. In this work, we report a series of hydrophobic and hydrophilic caged fluorophores that overcome the preceding limitations. Based on the robust pyranine backbone, they can easily be synthesized on a large scale in one to a few steps. Their brightness increases over illumination and their uncaging cross-sections have been thoroughly characterized upon one- and two-photon excitation. As a demonstration of their use, we calibrated light intensity in various chemical and biological samples, which have been observed with epifluorescence and confocal imaging systems.

Introduction

Light is a trigger and reactant, which is endowed with attractive features. Indeed, it is essentially non-invasive, can be delivered with exclusive temporal and spatial resolution, and be used as well for introducing a perturbation and reading out its impact. Moreover, many light sources are nowadays available to deliver various photon fluxes in different wavelength ranges. Light has accordingly found ubiquitous exploitation in many academic and applied fields of Chemistry (*e.g.* photocatalysis[1,2]), Biology (*e.g.* optogenetics[3–5]), Physics (*e.g.* fluorescence bioimaging[6]), and Engineering (*e.g.* decontamination,[7] measurement of environmental radiation[8–11]).

Despite its attractive features, light often suffers from the lack of characterization of its sources, which makes it difficult to compare the results obtained in various groups as well as to ensure reproducibility. Light meters in which a detector integrates the overall photon flux over an illuminated surface are not often available in the laboratories of Chemistry and Biology.[12,13] Moreover, their proper use requires technical expertise and they do not give direct access to the photon flux density (irradiance). In contrast, actinometers can yield the photon flux density at a sample from analyzing the time dependence of the extent of their photoconversion.[14,15] However, most of them rely on absorbance for reporting, which is not sensitive enough to measure light intensity in tiny samples (*e.g.* for calibrating the illumination of microscopes). Fluorescent actinometers are attractive to overcome this limitation.

Most photoactivatable fluorophores switch from a dark to a bright state under illumination. Obtained by grafting a caging group which acts as a fluorescence quencher[16–18] or as a dark precursor in which fluorescence is restored upon light irradiation,[19–24] they have been exploited in numerous fields (*e.g.* investigation of cell lineage,[25,26] spatiotemporal interrogation of fluid flows,[27] reconstruction of images with subdiffraction resolution[28,29]). However, they have only been sporadically characterized in order to yield quantitative information on the absolute value of the light intensity.[23,30–34] Importantly, the task of measuring light intensity is not restricted to one-photon excitation. Indeed, two-photon excitation is currently used both in fluorescence imaging (where it benefits from intrinsic excellent spatial resolution) and in optogenetics (for local photoactivation). Since it relies on focusing light from a high laser power, it is crucial to get information on the light intensity at the sample to obtain the desired two-photon-driven excitation while avoiding any detrimental impact of illumination. Hence, in this manuscript, we report the design, the syntheses, and the characterization of a whole series of hydrophobic, hydrophilic, and cell-permeant caged fluorophores, which are subsequently implemented to calibrate light intensity with one-

[a]PASTEUR, Département de chimie, École normale supérieure, PSL University, Sorbonne Université, CNRS, 24, rue Lhomond, 75005 Paris, France. E-mail: Isabelle.Aujard@ens.psl.eu; Thomas.Lesaux@ens.psl.eu; Ludovic.Jullien@ens.psl.eu

[b]Laboratoire des biomolécules (LBM), Département de chimie, École normale supérieure, PSL University, Sorbonne Université, CNRS, 24, rue Lhomond, 75005 Paris, France

† Electronic supplementary information (ESI) available. See DOI: https://doi.org/10.1039/d3sc04183b

and two-photon excitation in various environments and under different geometries.

Results and discussion

Principle

We consider a caged fluorophore. It is first suddenly submitted to spatially homogeneous and time-constant illumination with one-photon excitation set at the level of light intensity I to be measured. Provided that the absorbance of its solution is lower than 0.15, the light intensity is then essentially constant along the optical path. When its photoactivation is rate-limiting, the time evolution of its fluorescence emission reporting its photoconversion extent can be reliably fitted with a monoexponential function. Under such a condition, the retrieved characteristic time τ gives access to the light intensity I which is given in eqn (1)

$$I = \frac{1}{\sigma\tau} \quad (1)$$

where σ is the photoconversion cross-section with one-photon excitation.

Accessing light intensity with two-photon excitation further requires to know the beam waist ω_{xy} of the focused laser in order to get geometrical information. Then monoexponentially fitting the time evolution of the fluorescence signal from the illuminated solution of the caged fluorophore in a container (*e.g.* a microchamber or a cell) yields a characteristic time, which can be converted in the light power P at the sample with eqn (2).

$$P = \left[\frac{\tau_P}{0.737\tau\delta T}\left(\frac{\pi hc\omega_{xy}}{\lambda}\right)^2\left(\frac{V}{V_{exc}}\right)\right]^{0.5} \quad (2)$$

In eqn (2), τ_P, h, c, δ, T, λ, V, and V_{exc} denote the duration of the laser pulses, the Planck constant, the light velocity in a vacuum, the cross-section for two-photon uncaging, the period of the laser pulses, the excitation wavelength, the volume of the container, and the focal volume resulting from laser focusing, respectively.

Design of the caged fluorophores

As a fluorophore scaffold, we chose 8-hydroxypyren-1,3,6-trisulfonic acid (HPTS, pyranine). This bright fluorophore is commercially available and highly water soluble, and it has found a wide range of applications as a tracer[35,36] or as a pH indicator with a pK_a equal to 7.3.[37] After activation of the sulfonic groups, HPTS can be derivatized using nucleophiles to yield sulfonic esters and sulfonamides.[38] In this work, we are interested to produce caged pyranine derivatives, which were anticipated to exhibit a range of solubility properties.

HPTS itself has already been derivatized with a photolabile protecting group to produce caged fluorophores. The uncaging features of its 1-(2-nitrophenyl)ethyl ether[30] have been established with one-[30,31] and two-[32] photon excitation. Its 4,5-dimethoxy-2-nitrobenzyloxy ether has also been reported in a patent.[39] However, the reported syntheses of these caged ethers required tedious purification steps. In this manuscript, we first adopted the 4,5-dimethoxy-2-nitrobenzyl caging group, which benefits from a more red-shifted absorption than the 2-nitrobenzyl one so as to absorb light in a wavelength range useful for many applications. For the purpose of comparison, we also investigated the 6,7-dimethoxycoumarinyl-4-methyl caging group, which exhibits similar light absorption properties but a distinct mechanistic pathway for uncaging.[17] The corresponding caged HPTS **NPy-S** and **CPy-S** (see Chart 1) have been produced with an efficient one-step synthetic protocol, which is compatible with the production of large amounts without any chromatography. Then **NPy-S** and **CPy-S** uncaging has been quantitatively characterized with one- and two-photon excitation and subsequently used for calibrating the light intensity of a confocal microscope.

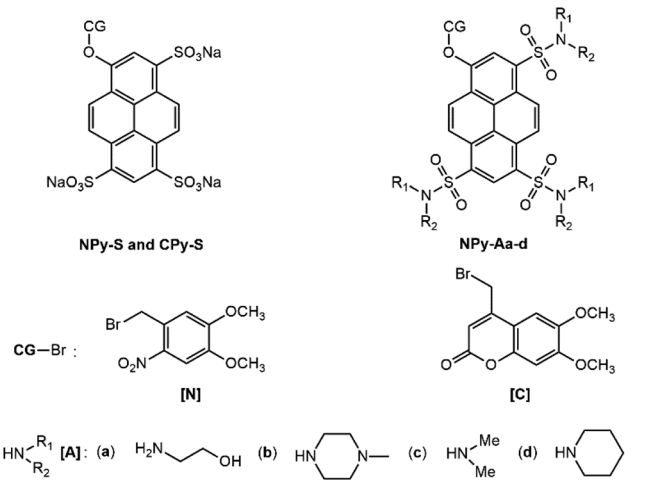

Chart 1 Chemical structures of the caged pyranine derivatives **NPy-S**, **CPy-S**, and **NPy-Aa-d**.

The caged HPTS derivatives contain three ionizable sulfonic acid groups. Hence, they are well suited for applications in aqueous solutions. In contrast, they cannot be used for biological applications requiring internalization into cells nor in organic solvents. To overcome this limitation, we produced trisulfonamide pyranines, which have been caged with the 4,5-dimethoxy-2-nitrobenzyl group (see Chart 1). To favor water solubility while enabling crossing of the cell bilayers, we adopted the ethanolamino and *N*-methylpiperazino sulfonamide substituents, which possess some organic characteristics but as well traits favoring water-solubility either mediated by hydrogen bonding or generation of positive charges by protonation. Hence, we targeted the corresponding caged pyranine derivatives **NPy-Aa** and **NPy-Ab**. To achieve solubility in organic solvents while generating various steric hindrances to modulate any possible aggregation of the pyrene backbone, we chose dimethylamino and piperidino sulfonamide substituents and targeted the caged trisulfonamide pyranine derivatives **NPy-Ac** and **NPy-Ad**. We herein report the syntheses of these caged pyranine derivatives, their uncaging properties, and their application for measuring light intensity in living cells and zebrafish embryos.

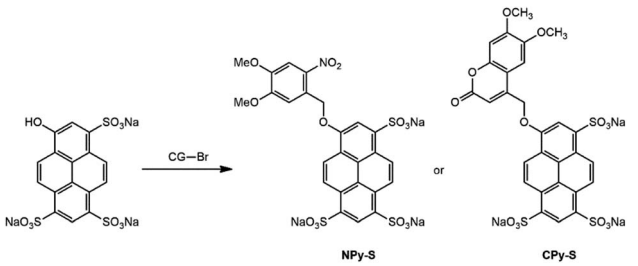

Scheme 1 Syntheses of the caged HPTS **NPy-S** and **CPy-S**.

Syntheses

The caged HPTS **NPy-S** and **CPy-S** have been synthesized in one step with 90% and 74% respective yields upon etherifying the HPTS phenol with 4,5-dimethoxy-2-nitrobenzylbromide and 6,7-dimethoxy-4-bromomethyl coumarin (Scheme 1).

The caged trisulfonamide pyranine derivatives were synthesized in four steps (Scheme 2a). In the first step, ester **1** was produced in 92% yield from acylating the HPTS phenol with acetic anhydride.[35] In the next step, its sulfonic acid groups were converted to chlorosulfonyl groups by reacting with oxalyl chloride to form compound **2**, which was used for the next step without any further purification.

The free trisulfonamide pyranine derivatives **Py-Aa-d** were then obtained by condensation of compound **2** with the amines in fair to good yields (50–71%). Then the caged trisulfonamide pyranine derivatives **NPy-Aa-d** were synthesized by reacting the free pyranine derivatives **Py-Aa-d** with 4,5-dimethoxy-2-nitrobenzylbromide in the presence of potassium carbonate in 54–80% yield. Alternatively, the caged trisulfonamide pyranine derivative **NPy-Ad** was obtained in 50% yield from converting the sulfonic acid groups of **NPy-S** to chlorosulfonyl groups with oxalyl chloride, followed by reaction with piperidine (Scheme 2b). It is noteworthy that none of these syntheses requires any dedicated separation nor tedious purification. In this respect, the pathway starting from the **NPy-S** caged HPTS enables the elimination of any residual free fluorophore **Py-Ad** in the final caged pyranine derivative **NPy-Ad**.

First investigations

All the free or caged pyranine derivatives are readily soluble in dimethyl sulfoxide to produce stock solutions. Hence, they were first dissolved in dimethyl sulfoxide and then diluted in their

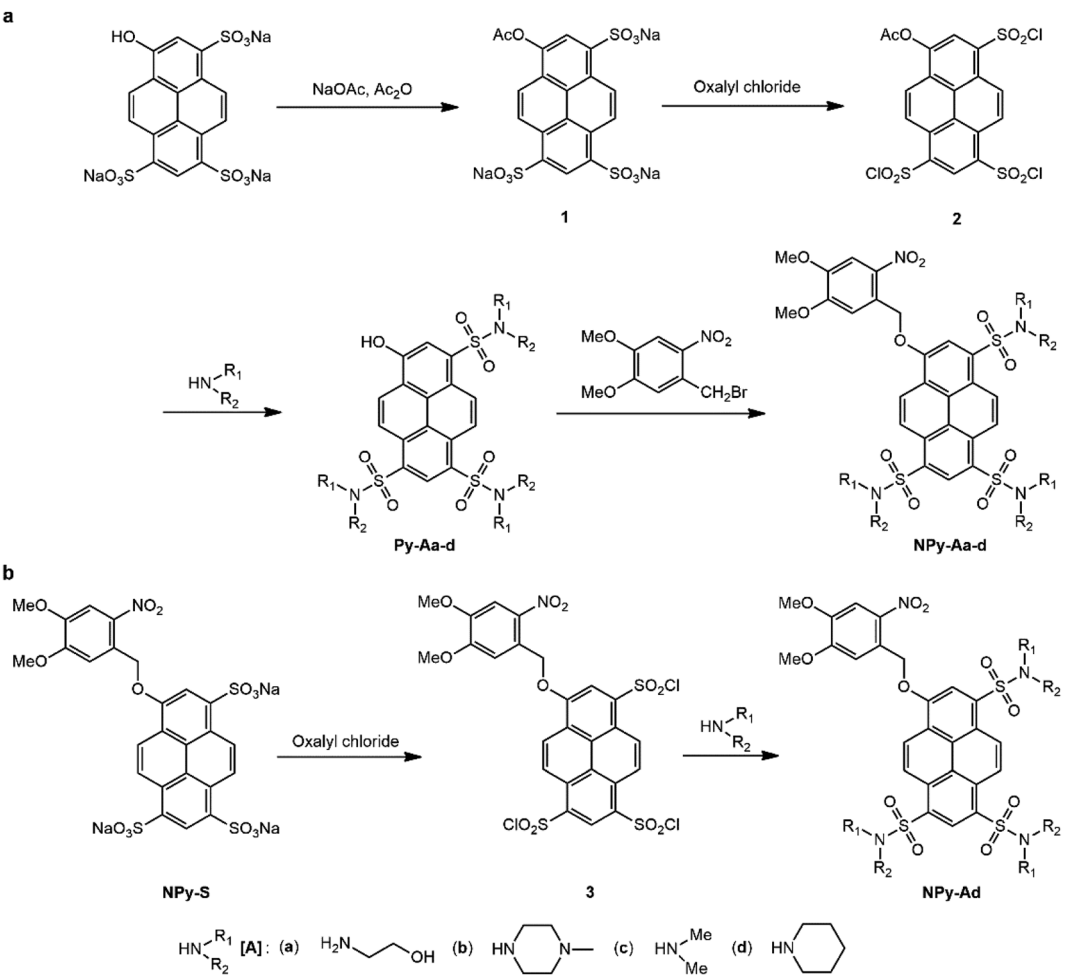

Scheme 2 Syntheses of the caged pyranine derivatives **NPy-Aa-d** from HPTS (a) or **NPy-S** (b).

Table 1 Absorption and emission properties of the free (**Py-Aa-d** and **HPTS**) and caged (**NPy-Aa-d**, **NPy-S**, and **CPy-S**) pyranine derivatives. λ_{abs}^{max}, $\varepsilon(\lambda_{abs}^{max})$, and λ_{em}^{max} denote the maximum of light absorption, the molar absorption coefficient at λ_{abs}^{max}, and the maximum of fluorescence emission respectively. Solvents: 10 mM pH = 7.4 PBS buffer (for **Py-Aa-b** and **NPy-Aa-b**), 1 mM pH = 8.4 Trizma buffer/acetonitrile 1/19 (v/v) (for **Py-Ac-d** and **NPy-Ac-d**), and 10 mM pH = 8.4 Trizma buffer (for **HPTS**, **NPy-S** and **CPy-S**)

Pyranine derivatives	λ_{abs}^{max} (nm)	$\varepsilon(\lambda_{abs}^{max})$ (mM^{-1} cm^{-1})	λ_{em}^{max} (nm)
Py-Aa	489	29	545
NPy-Aa	421	9	538
Py-Ab	500	23	552
NPy-Ab	432	21	543
Py-Ac	522	10	556
NPy-Ac	417	39	—[a]
Py-Ad	524	10	557
NPy-Ad	419	36	—[a]
HPTS	456	24	507
NPy-S	401	17	507
CPy-S	401	25	510

[a] Too weak to be reliably evaluated.

Table 2 Photoconversion parameters of **NPy-Aa-d**, **NPy-S**, and **CPy-S**. σ_I, σ_{II}, and σ_{III}, respectively denote the uncaging cross-sections of the caged pyranine derivatives extracted from analyzing (i) the time dependence of the rise of the fluorescence emission at 540 nm for solutions of **NPy-Aa-d**, at 500 nm for the solution of **NPy-S**, and at 510 nm for the solution of **CPy-S** under monochromatic illumination at 365 nm; (ii) the light intensity-dependence of the inverse of the associated characteristic time τ for **NPy-Ab**, **NPy-Ad**, **NPy-S** and **CPy-S** at 365 nm; (iii) the time evolution of the concentrations in caged pyranine derivative and its photoreleased free pyranine derivative measured by capillary electrophoresis (for **NPy-Ab**) and HPLC (for **NPy-Ad**, **NPy-S** and **CPy-S**) under illumination at 365 nm. T = 293 K

Pyranine derivatives	σ_I (m^2 mol^{-1})	σ_{II} (m^2 mol^{-1})	σ_{III} (m^2 mol^{-1})
NPy-Aa	1.6 ± 0.2	—	—
NPy-Ab	6.8 ± 0.7	6.2 ± 0.6	8.2 ± 0.8
NPy-Ac	18.3 ± 2.0	—	—
NPy-Ad	15.6 ± 1.6	38.9 ± 3.9	25.2 ± 2.5
NPy-S	8.4 ± 0.7	16.3 ± 1.6	6.0 ± 0.6
CPy-S	560 ± 56	462 ± 46	695 ± 70

respective solvents for all experimental studies. The hydrophilic free and caged pyranine derivatives were diluted either in 10 mM pH = 7.4 PBS buffer or 10 mM pH = 8.4 Trizma buffer for **NPy-Aa-b**, **NPy-S** and **CPy-S**. At the corresponding pH, the phenol group of the free pyranine derivative is fully ionized (*vide infra*). This results in maximizing the fluorescence emission upon 488 nm wavelength excitation, which is widely available on commercially available optical setups. The hydrophobic free and caged pyranine derivatives were generally diluted in 1 mM pH = 8.4 Trizma buffer/acetonitrile 1/19 (v/v) for **NPy-Ac-d**. Here the organic solvent enables good solubility whereas the presence of water is required to liberate the free pyranine derivative[17] and the basicity of the aqueous buffer causes phenol ionization of the free pyranine.

At neutral pH, the free pyranine derivatives **Py-Aa-d** exhibit a strong absorption band in the 440–550 nm wavelength range peaking at 500 nm, which is red-shifted by 50 nm in comparison to HPTS (see Fig. S3†). Upon decreasing pH, this absorption band drops and a new absorption band appears at 420 nm as anticipated from the gradual protonation of the phenolate yielding the phenol (see Fig. S4†). The dependence of the absorbance at 488 nm and 420 nm on pH was utilized to extract the ground state pK_a of the phenol function in the hydrophilic trisulfonamide pyranine derivatives **Py-Aa-b**. We found 6.0 ± 0.1 for **Py-Aa**, which is in reasonable agreement with reported values for pyranine trisulfonamides.[38] For **Py-Ab**, the dependence of the absorbance on pH was better accounted for by taking into account two proton exchange constants. We found 4.7 ± 0.1 and 6.6 ± 0.1, which are interpreted as arising from ionization of the phenol and a protonated *N*-methyl nitrogen respectively. The pK_a of **Py-Aa** is lower than the one of the parent HPTS (7.3 (ref. [37])) as anticipated from the absence of any destabilizing electrostatic interaction in the phenolate form. It is even lower in **Py-Ab** as expected from the stabilizing interaction between the negative charge of the phenolate and the positive charge of the ammonium. At neutral pH, the corresponding caged derivatives (**NPy-Aa-d**, **NPy-S**, and **CPy-S**) exhibit a maximum of absorption around 420 nm similar to the one observed for the phenol form of the free pyranine as expected from engaging its OH group in an ether linkage. All the spectroscopic parameters are reported in Table 1 (see also Table 3).

We next proceeded to a first series of preliminary illumination experiments to establish the relevance of the design of the caged pyranine derivatives **NPy-Aa-d**, **NPy-S**, and **CPy-S** and to fix optimal conditions for their reliable use as fluorescent actinometers for measuring light intensity. More precisely, we followed the time evolution of the fluorescence signal upon applying time constant and spatially homogeneous light at 365 nm on solutions of the caged pyranine derivatives (**NPy-Aa-d**, **NPy-S**, and **CPy-S**) contained in 54 μL cuvettes (3 mm optical pathlength). Fig. S5–S12† display the results. Depending on the nature of the caged pyranine derivative and on the experimental conditions, we observed an increase of the fluorescence signal by a factor of 1.4 to 20, which mainly occurred at the 50–500 s time scale at (0.1–2.5) 10^{-8} E s^{-1} light intensity and (0.6–14) 10^{-4} E m^{-2} s^{-1} photon flux density. We further evaluated 17–72% as the range of the uncaging yield from comparing the fluorescence intensities of solutions of the free pyranine derivatives (**Py-Aa-d** and **HPTS**) with the ones of solutions of the caged pyranine derivatives (**NPy-Aa-d**, **NPy-S**, and **CPy-S**) at the same concentration after uncaging. In particular we selected optimal experimental conditions in which the time evolution of the fluorescence signal of the illuminated solution could be reliably fitted with a monoexponential fitting function to extract the characteristic time τ, which led us to retrieve first values of the uncaging cross-sections σ from the knowledge of the applied light intensity I by using eqn (1) (see Table 2). In parallel, we performed experiments with biological samples with the caged pyranine derivatives **NPy-Aa-b**. We noticed that

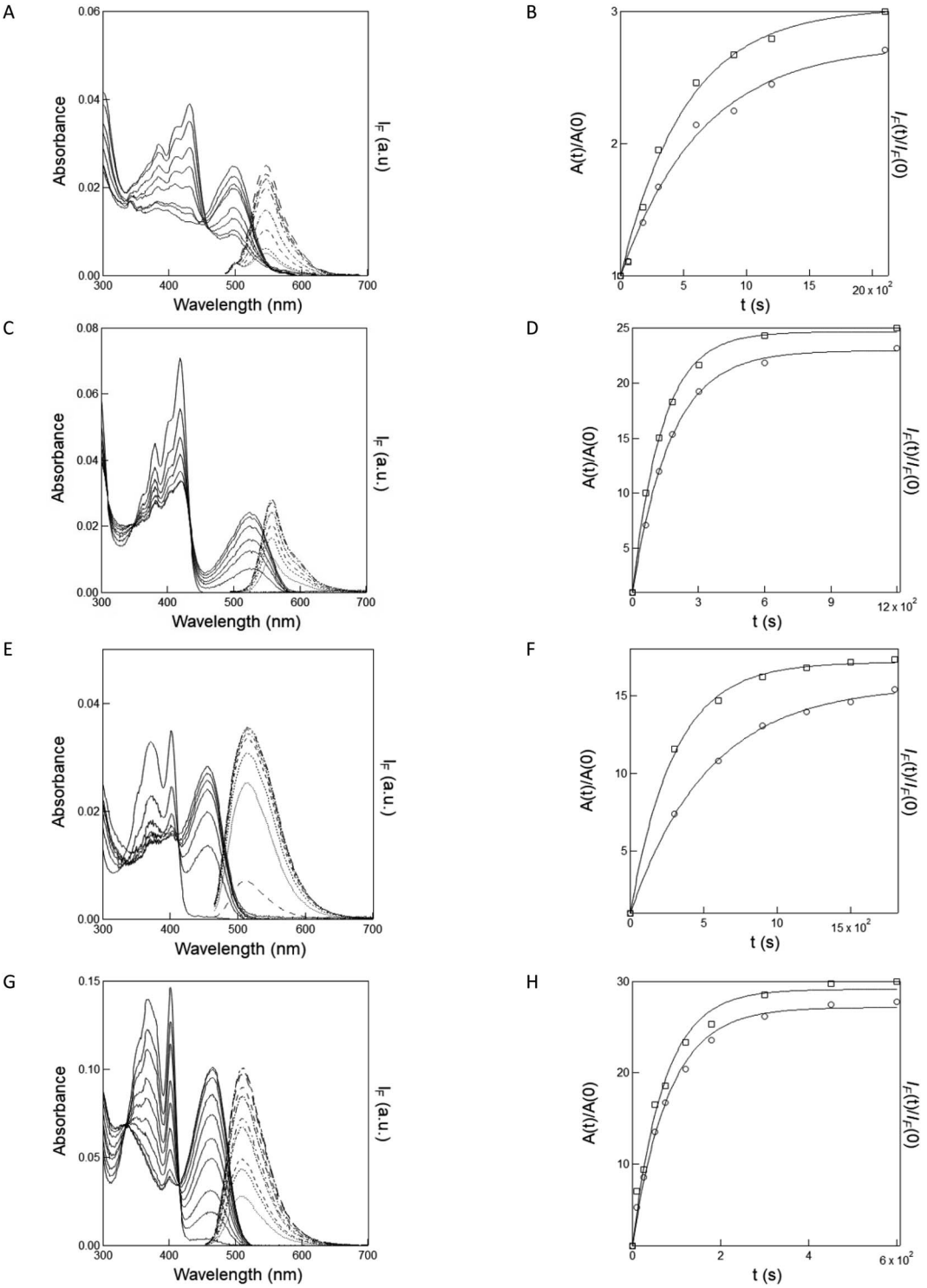

Fig. 1 Quantitative analysis of **NPy-Ab**, **NPy-Ad**, **NPy-S** and **CPy-S** uncaging at 365 nm from absorption and fluorescence reporting. (A, C, E, G) Time evolution of the absorption (solid lines) and emission (dotted lines; $\lambda_{exc} = 480$ nm in (A, C) and 450 nm in (E, G)) spectra of solutions contained in a 1×1 cm^2 quartz cuvette exposed to irradiation at 365 nm at constant light intensity I. (A) 2 μM **NPy-Ab** in 10 mM pH = 8.4 Trizma buffer, $I = 7.2 \times 10^{-8}$ E s^{-1}. Time (s): 0, 60, 180, 300, 600, 900, 1200, 2100; C: 2 μM **NPy-Ad** in 1 mM pH = 8.4 Trizma buffer/acetonitrile 1/19 (v/v), $I = 8.7\,10^{-8}$ E s^{-1}. Time (s): 0, 60, 120, 180, 300, 600, 1200; (E) 2 μM **NPy-S** in 10 mM pH = 8.4 Trizma buffer, $I = 7.2 \times 10^{-8}$ E s^{-1}. Time (s): 0, 300, 600, 900, 1200, 1800; (G) 5 μM **CPy-S** in 10 mM pH = 8.4 Trizma buffer, $I = 5.4 \times 10^{-9}$ E s^{-1}. Time (s): 0, 10, 25, 50, 75, 120, 180, 300, 450 and 600; (B, D, F, H): temporal evolution of the normalized absorbance (circles; λ_{abs}(nm): (B) 480; (D) 524; (F) 456; (H) 450) and normalized emission (squares; λ_{exc} (nm), λ_{em} (nm): (B) 480, 540; (D) 480, 556; (F), (H) 450,510). Markers: Experimental data from (A), (C), (E), (G), lines: monoexponential fit with eqn (S1).† Characteristic times have been retrieved from the absorbance and fluorescence data respectively: (B) 642 s and 515 s; (D) 173 s and 134 s; (F) 535 s and 298 s; (H) 82 s and 72 s. $T = 293$ K.

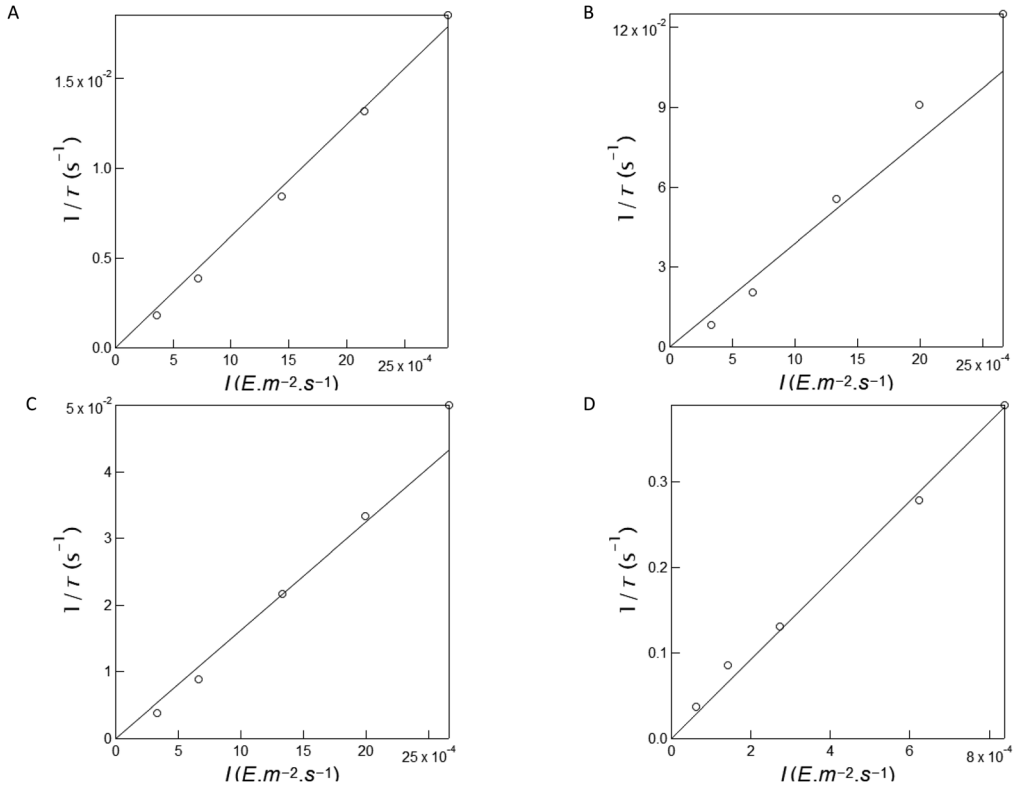

Fig. 2 Measurement of the uncaging cross-section of **NPy-Ab**, **NPy-Ad**, **NPy-S** and **CPy-S** at 365 nm. Light intensity-dependence of the inverse of the characteristic time τ retrieved from the monoexponential fit of the fluorescence rise under 365 nm illumination for **NPy-Ab** (A), **NPy-Ad** (B), **NPy-S** (C) and **CPy-S** (D) in Fig. S11a–d.† Markers: Experimental data; solid line: linear fit. The extracted slopes are 6.2, 38.9, 16.3 and 462 m^2 mol^{-1} for **NPy-Ab**, **NPy-Ad**, **NPy-S** and **CPy-S** respectively. $T = 293$ K.

we could not achieve any penetration of **NPy-Aa** in living cells even after a long incubation (see Fig. S18†), which led us to discard the latter caged pyranine derivative for further investigations.

As an outcome of this first series of experiments, we selected four caged fluorophores for further characterization making them relevant for calibration of light intensity in various environments: (i) **NPy-Ad** for applications in organic solvents and hydrophobic media; (ii) **NPy-S** and **CPy-S** for applications in aqueous solutions; (iii) **NPy-Ab** for biological applications requiring permeation through cell bilayers.

Quantitative analysis of uncaging of NPy-Ab, NPy-Ad, NPy-S and CPy-S with one-photon excitation

Fig. 1A, C, E and G display the time evolution of the absorption and emission spectra of the caged pyranine derivatives (**NPy-Ab**, **NPy-Ad**, **NPy-S** and **CPy-S**) upon illumination in a 1 × 1 cm^2 quartz cuvette with a LED emitting at 365 nm in 10 mM pH = 7.4 PBS, 1 mM pH = 8.4 Trizma buffer/acetonitrile 1/19 (v/v), and 10 mM pH = 8.4 Trizma buffer respectively.

As anticipated from uncaging at the considered pH, one observes the gradual decay of the absorption band associated with the caged pyranine derivatives **NPy-Ad**, **NPy-S** and **CPy-S** and the rise of the absorption band associated with the anionic form of the free pyranine **Py-Ad** and **HPTS**. The presence of isosbestic points further suggests the absence of any observable intermediate in the conversion of the caged into the free pyranine at the considered time scale.

As expected from caging the phenolic OH group, all the caged pyranine derivatives are weakly fluorescent or non-fluorescent upon excitation at 450–480 nm. Under illumination at 365 nm, one observes the gradual rise of the fluorescence emission identical to the one of the free pyranine, which supports the photorelease occurrence. We next analyzed the kinetics of the time evolutions of the absorbance and fluorescence signals. As shown in Fig. 1B, D, F and H, they were satisfactorily fitted with monoexponential functions and the extracted characteristic times were found in the same range for both observables. Hence, 642 and 515, 173 and 134, 535 and 298, and 82 and 72 s were found with absorbance and fluorescence for **NPy-Ab**, **NPy-Ad**, **NPy-S** and **CPy-S** respectively.

In a second series of experiments for quantitative characterization of the uncaging of **NPy-Ab**, **NPy-Ad**, **NPy-S** and **CPy-S**, we reproduced the experiments displayed in Fig. 1 upon irradiation at various light intensities delivered by a LED at 365 nm (see Fig. S13†). Then we applied the monoexponential fitting function given in eqn (S1)† to the temporal rises of the normalized fluorescence in order to retrieve the characteristic times of the photoconversion τ. As displayed in Fig. 2A–D, the

inverse of the characteristic times of the photoconversion linearly depends on the light intensity. This behavior demonstrates that the rate limiting step of uncaging is photochemical at least up to 15.6×10^{-8} E s^{-1} light intensity. A linear fit was used to retrieve the values of the uncaging cross-sections from the slope: 6.2, 38.9, 16.3 and 462 m^2 mol^{-1} were found for **NPy-Ab**, **NPy-Ad**, **NPy-S** and **CPy-S** respectively (see Table 2).

Equipped with the values of the uncaging cross-sections at 365 nm, we expanded the range of excitation wavelengths for uncaging by using a Xe lamp as a light source. Hence, we recorded the time evolution of the fluorescence signal from solutions of **NPy-Ab**, **NPy-Ad**, **NPy-S** and **CPy-S** upon applying illumination from 300 to 440 nm (see Fig. S14†). After monoexponential fitting, we retrieved the corresponding characteristic times, which were converted into values of the uncaging cross-section σ from knowledge of the light power measured with a power meter by further using the value of the uncaging cross-sections at 365 nm as a reference. The results are displayed in Table 3. Combined with the absorption spectra of **NPy-Ab**, **NPy-Ad**, **NPy-S** and **CPy-S** displayed in Fig. S3B, D and E,† they have been used to retrieve the uncaging quantum yields of **NPy-Ab**, **NPy-Ad**, **NPy-S** and **CPy-S** at several wavelengths (see Table 3).

The uncaging quantum yields of **NPy-Ab**, **NPy-Ad**, and **NPy-S** are in the expected range found for diverse substrates caged with the nitroveratryl group.[40] In contrast, one notices the high value of the uncaging quantum yield of **CPy-S**. Interestingly, non-vanishing quantum yields of uncaging are found for **NPy-Ab** and **NPy-Ad** at 440 nm at which wavelength the caging group does not significantly absorb.[40] This observation suggests that there is a coupling between the pyranine and the nitroveratryl chromophore for driving uncaging, which may also account for some variation of the extracted quantum yields with the excitation wavelength. This result is in line with previous observations in which coupling a chromophore with a caging nitrobenzyl group significantly altered the cross-section for uncaging of the latter with one-and two-photon excitation.[30,33]

In the last series of experiments for quantitative characterization of the uncaging of **NPy-Ab**, **NPy-Ad**, **NPy-S** and **CPy-S**, we measured their uncaging cross-section at 365 nm by using capillary electrophoresis or HPLC to quantitate both the disappearance of the caged pyranines and the formation of the photoreleased pyranine upon illumination at 365 nm. Fig. 3A–D display the results. As expected, the peak associated with the caged pyranine derivative gradually disappears and it tends towards zero. At the same rate, the peak from the free pyranine grows and saturates at concentrations indicating an uncaging yield in the (19–67)% range. After monoexponential fitting of the time concentration evolutions, we retrieved the characteristic times associated with the decay of the caged pyranine derivatives and the rise of the photoreleased pyranine derivatives and subsequently extracted the uncaging cross-sections: 8.2 ± 0.8, 28.9 ± 2.9 and 21.5 ± 2.1, 6.0 ± 0.6 and 6.0 ± 0.6, 606 ± 61 and 785 ± 78 m^2 mol^{-1} were respectively found for **NPy-Ab**, **NPy-Ad**, **NPy-S** and **CPy-S** in fair agreement with the values retrieved from the preceding fluorescence experiments (see Table 2).

We eventually ended up this series of uncaging experiments in cuvettes by evaluating the kinetics of photobleaching upon submitting 2 μM solutions of the free pyranine derivatives **Py-Ab**, **Py-Ad** and **HPTS** to LED illumination at 365 nm (see Fig. S15†). We could extract an estimate of their photobleaching cross-section: 0.7, 2.7, and 1.4 $m^2.mol^{-1}$ were retrieved for **Py-Ab**, **Py-Ad** and **HPTS** respectively, which suggests that no significant photobleaching should occur upon using the caged pyranine derivatives for measuring light intensity.

Table 3 Dependence of the photoconversion parameters of NPy-Ab, NPy-Ad, NPy-S and CPy-S on the wavelength of light excitation. The molar absorption coefficients $\varepsilon(\lambda)$ were retrieved from the spectra recorded at 2 μM concentration in 10 mM pH = 7.4 PBS buffer (for NPy-Ab), 1 mM pH = 8.4 Trizma buffer/acetonitrile 1/19 (v/v) (for NPy-Ad), and 10 mM pH = 8.4 Trizma buffer (for NPy-S and CPy-S) contained in a 1 × 1 cm^2 quartz cuvette. The uncaging cross-sections $\sigma(\lambda)$ of the caged pyranine derivatives have been extracted from analyzing the rise of the fluorescence emission at 540 nm of solutions of NPy-Ab and NPy-Ad, and at 510 nm of solutions NPy-S and CPy-S under monochromatic illumination at 300, 365, 405, and 440 nm as representatives of 300–440 nm range by further using the value of the uncaging cross-sections σ_{II} at 365 nm as a reference. The quantum yield of uncaging $\varphi(\lambda)$ of the caged pyranine derivatives has been extracted from the relation $\varphi(\lambda) = \sigma(\lambda)/[2.3\varepsilon(\lambda)]$. $T = 293$ K

Caged pyranine derivatives	λ_{exc} (nm)	$\varepsilon(\lambda)$ (mM^{-1} cm^{-1})	$\sigma(\lambda)$ (m^2 mol^{-1})	$10^3 \times \varphi(\lambda)$
NPy-Ab	300	24	2.6 ± 0.3	0.5 ± 0.1
	365	14	6.2 ± 0.6	1.9 ± 0.2
	405	18	1.4 ± 0.1	0.3 ± 0.02
	440	18	2.7 ± 0.3	0.7 ± 0.1
NPy-Ad	300	32	97.0 ± 9	13.2 ± 1.2
	365	17	38.9 ± 3.9	9.9 ± 1.0
	405	27	43.0 ± 4.3	6.9 ± 0.7
	440	4	9.2 ± 1	10 ± 1.1
NPy-S	300	6.5	29.1 ± 2.9	19.5 ± 1.9
	365	16	16.3 ± 1.6	4.4 ± 0.4
	405	16	4.7 ± 0.5	1.3 ± 0.1
CPy-S	300	10	544 ± 54	236 ± 23
	365	25	462 ± 46	80 ± 8
	405	22	464 ± 46	92 ± 9
	440	0.6	14 ± 1	101 ± 10

Quantitative analysis of uncaging of NPy-S and CPy-S with two-photon excitation

We also performed a series of experiments on **NPy-S** and **CPy-S** to measure their cross-section for uncaging with two-photon excitation. For designing the measurement protocol, we took advantage of the increase of the fluorescence signal upon uncaging. Fig. 4A and C respectively display the temporal evolution of the fluorescence emission from 3 μM solution of **NPy-S** and **CPy-S** in 10 mM pH = 8.4 Trizma buffer upon irradiation at 750 nm at (7–23) mW laser powers. One observes a continuous increase, which is in line with the realization of the uncaging process observed above. We retrieved the characteristic time τ from applying a monoexponential fitting function and we verified that the dependence of the inverse of τ with the applied laser power was quadratic as expected from

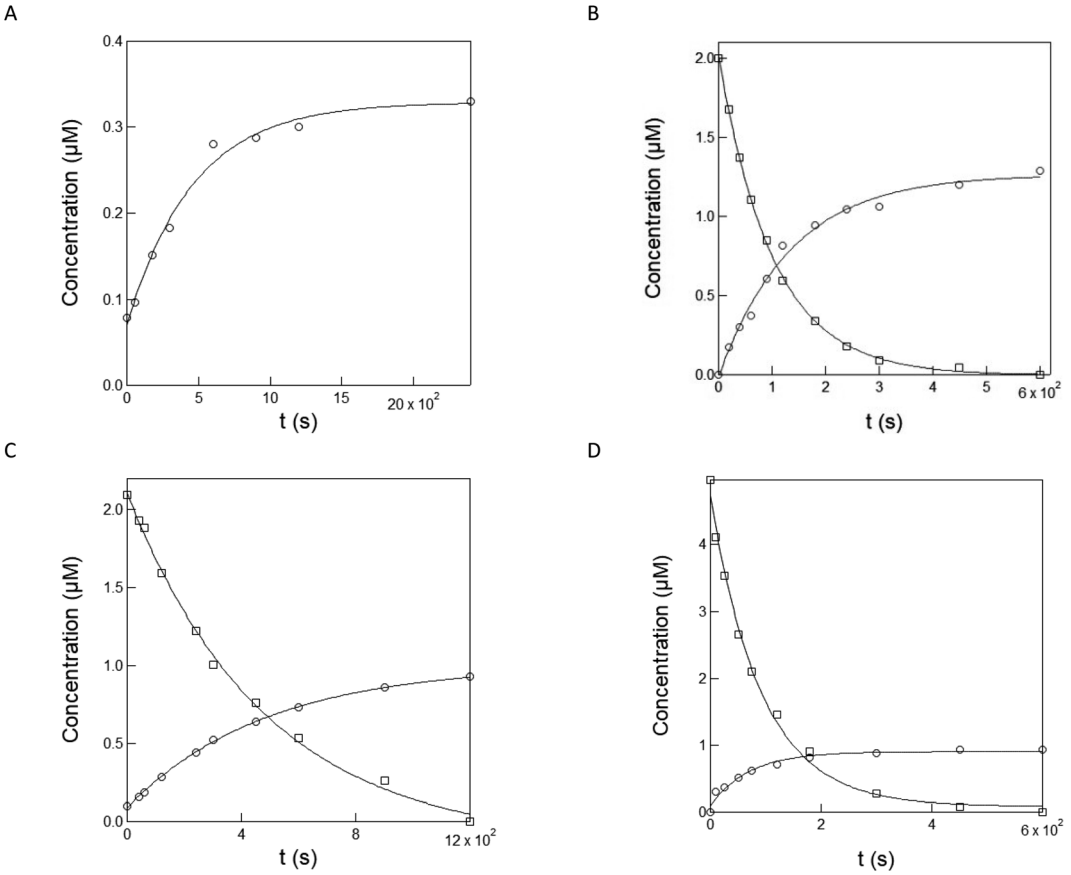

Fig. 3 Evaluation of the kinetics and yield associated with uncaging of **NPy-Ab** (by capillary electrophoresis), **NPy-Ad**, **NPy-S** and **CPy-S** (by HPLC) upon illumination at 365 nm LED. Time evolution of the composition of solutions of **NPy-Ab** ((A) 1 μM in 10 mM pH = 8.4 Trizma buffer), **NPy-Ad** ((B) 2 μM in 1 mM pH = 7.4 PBS buffer/acetonitrile 1/19 v/v), **NPy-S** ((C) 2 μM in10 mM pH = 8.4 Trizma buffer), and **CPy-S** ((D) 5 μM in 10 mM pH = 8.4 Trizma buffer) upon illumination at 365 nm at 1.0×10^{-7} E s^{-1} (for **NPy-Ab**, **NPy-Ad** and **NPy-S**) and 5.4×10^{-9} E s^{-1} (for **CPy-S**). Markers: concentrations of the caged compounds **NPy-Ad**, **NPy-S**, and **CPy-S** (squares) and photoreleased compounds **Py-Ab**, **Py-Ad** and **HPTS** (circles) as extracted from the peak areas in the electropherogram (for **NPy-Ab**) and HPLC chromatograms (**NPy-Ad**, **NPy-S** and **CPy-S**); solid lines: monoexponential fit with eqn (S1);† the characteristic times 101, 484, 92 s for **NPy-Ad**, **NPy-S** and **CPy-S** and 464, 136, 486, and 71 s for **Py-Ab**, **Py-Ad** and **HPTS** have been retrieved from (A), (B), (C) and (D) respectively. $T = 293$ K.

eqn (2). More precisely, we found 2.1 and 2.0 for the power exponent for **NPy-S** and **CPy-S** respectively. Hence, we could conclude that the observed uncaging behavior did result from two-photon absorption. We could also extract the associated uncaging cross-sections with two-photon excitation. We retrieved 4.2×10^{-3} and 4.2×10^{-2} GM for **NPy-S** and **CPy-S** respectively. In particular, the uncaging cross-section with two-photon excitation found for **NPy-S** compares well with the 4×10^{-3} GM value, which we previously found for another nitroveratryl caged phenol.[41]

Applications

As a first application, we implemented the caged pyranine derivative **NPy-Ab** for measuring light intensity in cultured cells. Living HeLa and HEK cells were conditioned for 30 min with 0.5 or 1 μM solutions of **NPy-Ab** in DMEM medium without generating any significant cell death (Fig. S16†). Their external medium was subsequently washed prior to illumination to avoid any possible interference, which could originate from photoreleasing the free fluorophore in the incubating solution. Then the HeLa and HEK cells were imaged with an epifluorescence by using 405 nm LED illumination. Fig. 5 displays the results. As shown in Fig. 5A and C, both cells conditioned with DMEM medium only did not yield any rise of the fluorescence emission upon illumination with a 405 nm LED. In contrast, we evidenced a rise of the fluorescence emission within 0.5 (Fig. 5B and D) or 1 (Fig. S17†) μM **NPy-Ab**-conditioned cells, which significantly departed from the corresponding behavior observed in the background and was consistent with the photorelease of free **Py-Ab** (see also Fig. S18† for a similar observation with 365 nm LED illumination). Moreover, we observed that the characteristic times retrieved from processing the fluorescence increase with a monoexponential function from illuminated cells under identical illumination conditions were essentially similar (0.21 and 0.23 s for HeLa and HEK cells respectively) and independent of the concentration of the **NPy-Ab** solution (0.21 and 0.28 s (in HeLa cells); 0.23 and 0.21 s (in HEK cells) for 0.5 and 1 μM respectively) (Fig. 5; see also Fig. S17†). Hence, we could adopt the uncaging cross-section of

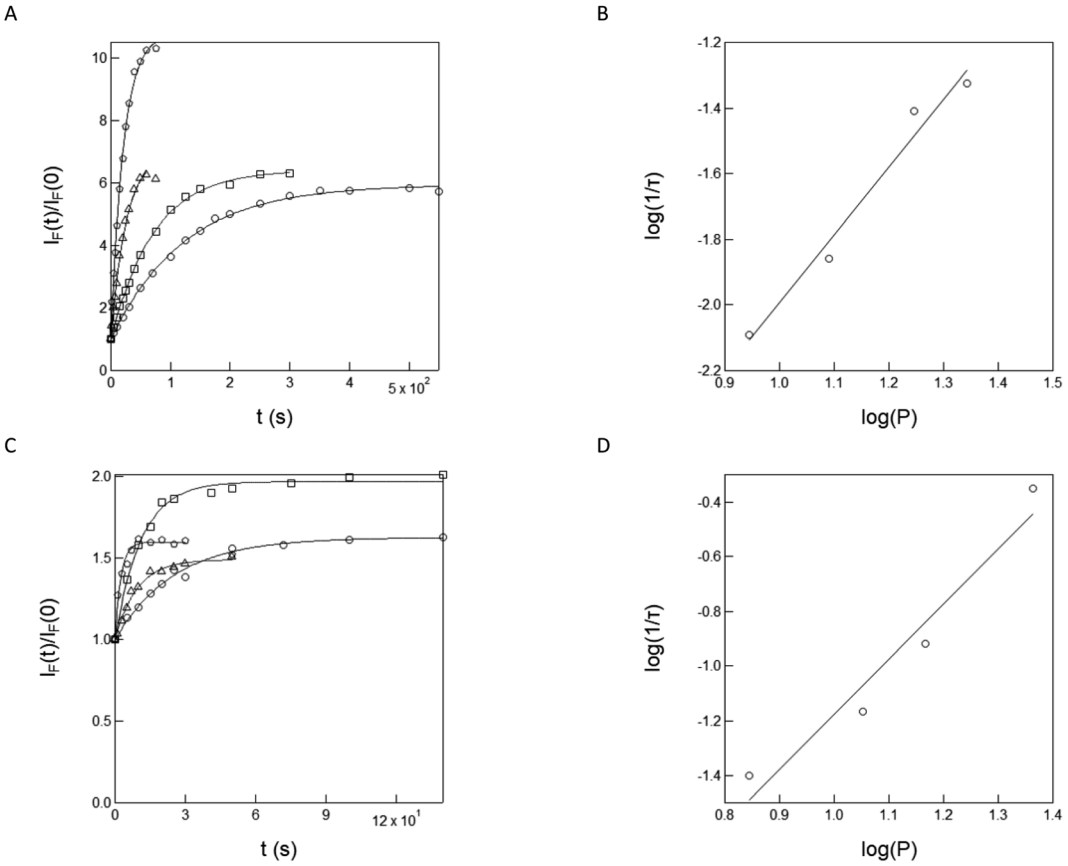

Fig. 4 Evaluation of the kinetics of uncaging for **NPy-S** and **CPy-S** with two-photon activation. Temporal evolution of the normalized fluorescence emission from 3 μM solutions of **NPy-S** (A) and **CPy-S** (C) in 10 mM pH = 8.4 Trizma buffer upon irradiation at $\lambda = 750$ nm at laser powers P (mW), 8.8 (circles), 12.3 (squares), 17.6 (triangles) and 22.0 (pentagons) for **NPy-S** and 7 (circles), 11.3 (disks), 14.7 (triangles) and 23.1 (pentagons) for **CPy-S**; dependence of the inverse of the characteristic time τ retrieved from the time evolutions displayed in (A) and (C) on the applied laser power P for **NPy-S** (B) and **CPy-S** (D). From the linear fits applied in B and D (solid lines), we retrieved the power exponent and the uncaging cross-sections with two-photon excitation from the slope and the intercept at the origin respectively. $T = 293$ K.

NPy-Ab in 10 mM pH = 8.4 Trizma buffer to extract the value of the photon flux density applied on both the cells and found 0.48 and 0.44 E m^{-2} s^{-1} for HeLa and HEK cells respectively under a 405 nm LED (and 0.1 E m^{-2} s^{-1} for HeLa cells under a 365 nm LED in Fig. S18†).

The preceding series of experiments have been performed at photon flux densities reaching at most 10^{-1} E m^{-2} s^{-1}. Such values are significantly lower than the ones currently exploited in high performance optical microscopies. Hence, we utilized the caged pyranine derivative **NPy-Ab**, **NPy-S** and **CPy-S** in order to explore the possibility of measuring the light intensity of a confocal microscope, which exploits photon flux densities up to 10^4 E m^{-2} s^{-1}. They were conditioned as liquid thin films sandwiched between two glass slides and submitted to dual illumination at 405 nm (for uncaging) and 488 nm (inactive for uncaging but favorable for imaging the photoreleased fluorophore). As displayed in Fig. 6A–C, the illumination governs an increase of the fluorescence intensity, which is in line with photoreleasing the free pyranine derivatives. We also retrieved the characteristic time τ from the time evolution of the fluorescence signals, from which we could extract 9.8, 4.3, and 444 m^2 mol^{-1} for the uncaging cross-section at 405 nm of **NPy-Ab**, **NPy-S** and **CPy-S** respectively from further exploiting the applied light power (independently measured with a power meter) and the beam waist of the 405 nm laser in the focal plane (see ESI†). The latter values of the uncaging cross-sections are in the range measured from the previous cuvette experiments (see Table 3). Hence the reasonable agreement between the values of the uncaging cross-sections over a wide range of photon flux densities suggests that the three caged pyranines **NPy-Ab**, **NPy-S** and **CPy-S** can be implemented to extract the photon flux density in a variety of optical setups. Specifically, we subsequently used the 9.8 m^2 mol^{-1} uncaging cross-section for **NPy-Ab** measured in confocal microscopy together with eqn (1) to retrieve the light intensity I in epifluorescence and confocal microscopy in biological systems.

As a demanded application in the context of optogenetics, we then exploited the caged pyranine derivative **NPy-Ab** for measuring light intensity delivered at 405 nm from a confocal microscope in living HeLa, HEK and zebrafish embryos.

In the absence of any control of the internal concentration in **NPy-Ab** within these systems, we preliminarily studied its significance in the uncaging kinetics. Fig. S7† shows that the characteristic times extracted for **NPy-Ab** uncaging at the same

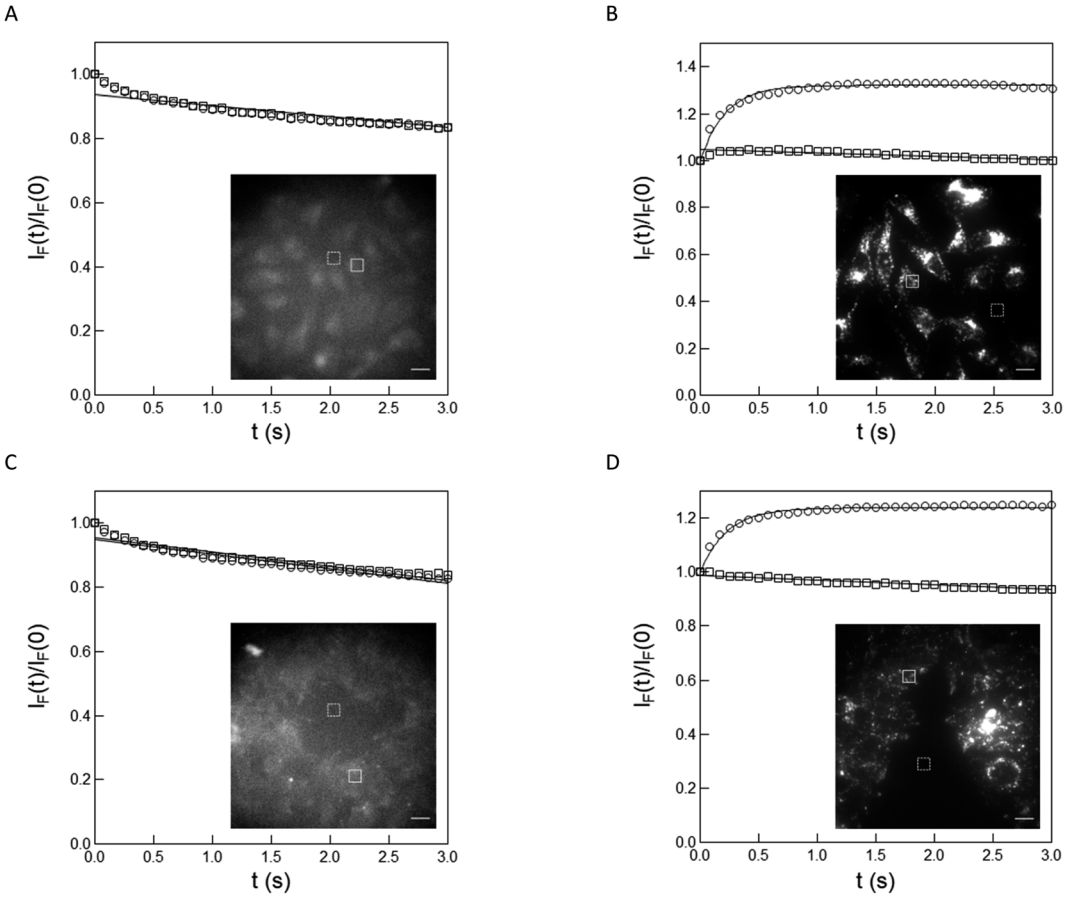

Fig. 5 Measurement of the photon flux density in living HeLa and HEK cells at 405 nm in epifluorescence microscopy. Time evolution of the fluorescence signal from living HeLa (A), (B) and HEK (C), (D) cells (inset; scale bar: 20 μm) conditioned with **DMEM** ((A), (C); control experiment) and 0.5 μM **NPy-Ab** (B), (D) under illumination at 405 nm. Markers: the circles and squares are associated with the frames delimited by the solid and dashed lines in the inset images respectively. Fluorescence signal as extracted from integrating the fluorescence level over the ROIs; solid lines: monoexponential fit with eqn (S1);† the characteristic times 0.21 and 0.23 s have been retrieved from processing the fluorescence signal over the frames delimited by the solid line in (B) and (D) respectively. $T = 298$ K.

15.6×10^{-9} E s^{-1} light intensity were similar at different concentrations spanning the 0.5–2 μM range thereby suggesting the **NPy-Ab** uncaging cross-section to be not dependent on its concentration within the investigated range.

We first examined the measurement of light intensity in living HeLa and HEK cells. Living cells conditioned with DMEM medium did not promote any fluorescence emission rise upon illumination at 405 nm (Fig. 6D and G). In contrast, a fluorescence rise satisfactorily fitted with a monoexponential function was observed in both HeLa and HEK cells incubated for 30 min with 1 μM **NPy-Ab** solution in DMEM medium and then washed with DMEM medium to avoid uncaging any external **NPy-Ab** (Fig. 6E and H; see also Fig. S19†). The latter observation was in line with the photo-release without any significant leakage through the cell membrane of the free pyranine derivative **Py-Ab** (see Fig. S20†). Using 9.8 m^2 mol^{-1} for the uncaging cross-section of **NPy-Ab**, we converted the distribution of characteristic times τ into the distribution of light intensity with 5.1×10^3 and 4.8×10^3 E m^{-2} s^{-1} average for living HeLa and HEK cells respectively (Fig. 6F and I).

These results allow us to measure the light intensity within the living cultured cells or zebrafish embryos without interference of diffusion of free **Py-Ab**.

We then proceeded with the measurement of light intensity in 5 hpf zebrafish embryos conditioned overnight with 1 μM **NPy-Ab** in water and then washed with water to remove any external **NPy-Ab** (see also Fig. S21†). They were placed in an agarose mold prior to light scanning with a confocal microscope under illumination at 405 nm. In the control experiment shown in Fig. 6J, illumination of **NPy-Ab**-free embryos did not promote any rise of the fluorescence emission. In contrast, the fluorescence signal rose upon illumination for the embryos conditioned with 1 μM **NPy-Ab** (Fig. 6K), which suggested **NPy-Ab** uncaging to occur with release of the free pyranine derivative **Py-Ab** (similar observations were made for embryos conditioned with 0.1 or 2 μM **NPy-Ab**; see Fig. S21†). We retrieved the characteristic times τ from applying a monoexponential function on the time evolutions of the fluorescence signal. Exploiting the 9.8 m^2 mol^{-1} uncaging cross-section of **NPy-Ab** measured in confocal microscopy and eqn (1), we then extracted the distribution of light intensity I in

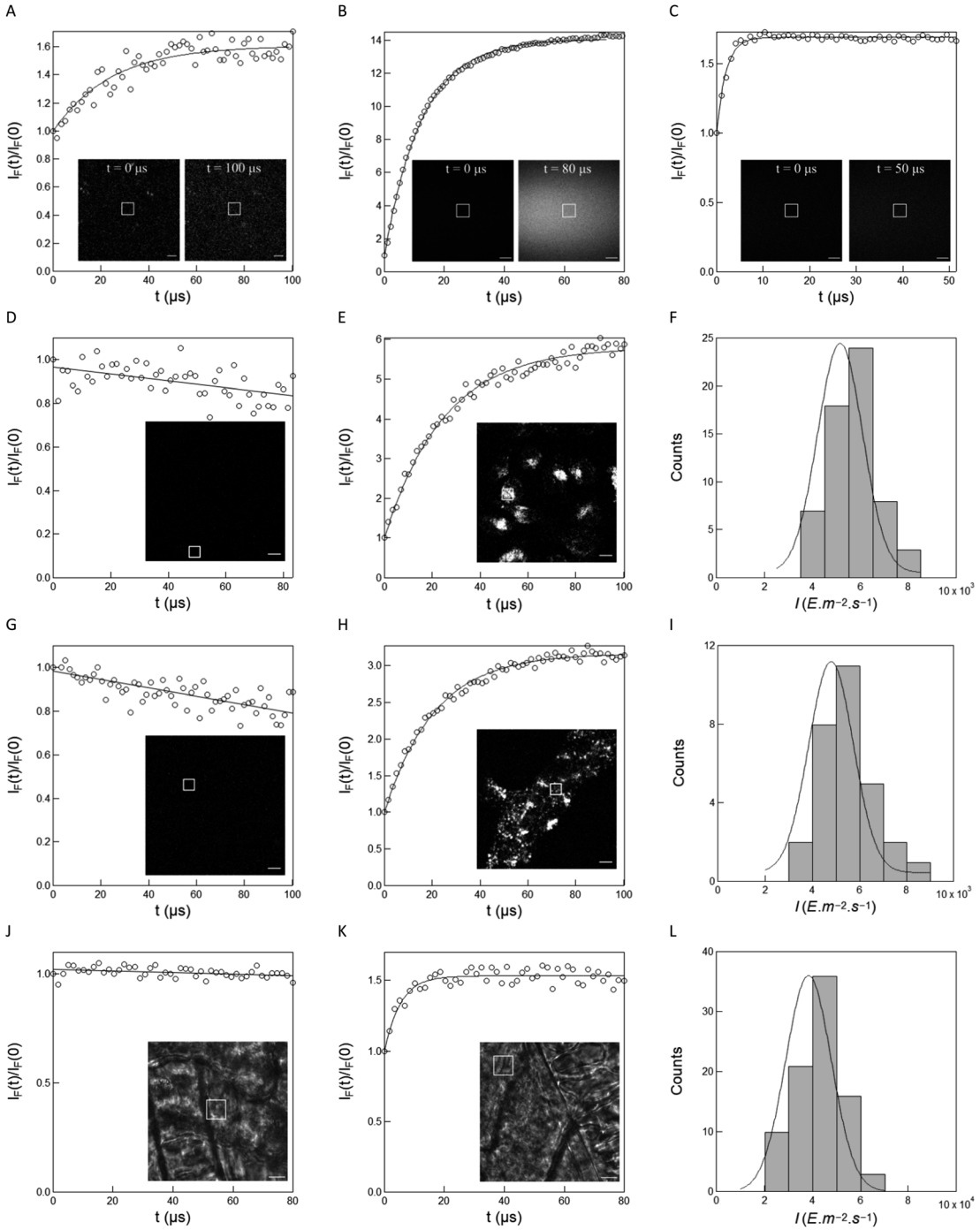

Fig. 6 Measurements of the photon flux density delivered at 405 nm in confocal microscopy. (A–C) Time evolution of the fluorescence signal from a liquid film (inset; scale bar: 10 μm for (A), and 50 μm for (B) and (C)) of 1 μM **NPy-Ab** in 10 mM pH = 8.4 trizma buffer (laser power: 2% for 405 nm; frame: 256 × 256 pixel^2; zoom factor: 4; dwell time: 1.7 μs) (A), 1 μM **NPy-S** in 10 mM pH = 8.4 Trizma buffer (laser power: 20% for 405 nm and 100% for 488 nm; frame: 1024 × 1024 pixel pixel^2; zoom factor: 1; dwell time: 1.03 μs) (B) and 2 μM **CPy-S** in 10 mM pH = 8.4 Trizma buffer (laser power: 1% for 405 nm and 100% for 488 nm; frame: 1024 × 1024 pixel pixel^2; zoom factor: 1; dwell time: 1.03 μs) (C) and of living HeLa (D, E) and HEK (G, H) (laser power: 2%; frame: 256 × 256 pixel pixel^2; zoom factor: 4; dwell time: 1.7 μs) and fluorescence image (inset; scale bar: 10 μm) cells conditioned with DMEM (D, G; control experiment) and 1 μM **NPy-Ab** (E, H; together with 2 μM DMSO originating from the **NPy-Ab** stock solution) in DMEM, and of living zebrafish embryos (J, K) (laser power: 10%; frame: 256 × 256 pixel^2; zoom factor: 5; dwell time: 1.7 μs) and bright field image (inset; scale bar: 10 μm) conditioned with 2 μM **DMSO** (J; control experiment) and 1 μM **NPy-Ab** (K; together with 2 μM DMSO originating from the **NPy-Ab** stock solution) in water. Markers: Fluorescence signal as extracted from integrating the fluorescence level over the ROI (white frame in the inset image); solid line: monoexponential fit with eqn (S1);† the characteristic time (μs) has been retrieved from processing the fluorescence signal over the ROI. A: 24; B: 13; C: 2; D: 25; H: 21; K: 5.3; F, I, L: distribution of light intensity I in living HeLa (F) and HEK (I) cells, and in living zebrafish embryos (L) conditioned with 1 μM **NPy-Ab** in DMEM (F, I) and water (L). Bars: Frequency of light intensity extracted from different ROIs (F: sample size: 60 ROIs, minimum/maximum bin: $3.0 \times 10^3/8.0 \times 10^3$ E m^{-2} s^{-1} and bin size: 1.0×10^3 E m^{-2} s^{-1}; I: sample size: 29 ROIs, minimum/maximum bin: $2.5 \times 10^3/8.0 \times 10^3$ E m^{-2} s^{-1} and bin size: 1.0×10^3 E m^{-2} s^{-1}; L: sample size: 88 ROIs from 10 embryos, minimum/maximum bin: $1.5 \times 10^4/7.0 \times 10^4$ E m^{-2} s^{-1} and bin size: 1.0×10^4 E m^{-2} s^{-1}); Solid lines: Fit with Eq. $f(x) = y_0 + A\exp\{-[(x - x_0)/w]^2\}$. $T = 293$ K.

living zebrafishes peaking at 3.8×10^4 E m^{-2} s^{-1} average value (Fig. 6L).

Conclusions

This report introduces and quantitatively characterizes the photoactivation properties of easily accessible caged fluorophores, which could find applications in multiple communities of end-users. We first set up syntheses of both hydrophilic and hydrophobic caged pyranine derivatives, which can be performed on a large scale and do not require any dedicated separation nor tedious purification. The resulting dark caged pyranine derivatives have been shown to liberate the corresponding fluorescent pyranines in a diversity of media upon illumination. Thus, a solution of caged pyranine absorbing constant light delivers a fluorescence signal, the time evolution of which can be robustly fitted with a monoexponential function. From extracting the characteristic time at known light intensities, we retrieved the associated uncaging cross-sections over a wide window of wavelengths and a broad range of light intensities. Equipped with this information, the present caged pyranine derivatives can be conversely harnessed for measuring light intensity with UV light in the 300–450 nm and 750 nm wavelength range with one and two-photon excitation respectively. In particular, we demonstrated their relevance for applications in aqueous solutions, hydrophobic solvents, and biological samples.

Data availability

Data for this paper, including the absorption spectra of the caged pyranine derivatives are available at Zenodo at **https://zenodo.org/doi/10.5281/zenodo.10137354**.

Author contributions

Conceptualization: I. A., T. L. S., L. J.; formal analysis: M. M., H. S. T., Q. M., E. S., I. A., T. L. S., L. J.; funding acquisition: I. A., T. L. S., L. J.; investigation: M. M., H. S. T., Q. M., E. S., M.-A. P., I. A., T. L. S., C. R., S. V.; methodology: M. M., I. A., T. L. S., L. J.; project administration: L. J.; resources: M. M., H. S. T., Q. M., E. S., M.-A. P., I. A., T. L. S., C. R., S. V.; supervision: I. A., T. L. S., L. J.; validation: M. M., H. S. T., Q. M., I. A.; visualization: M. M., H. S. T., I. A., L. J.; writing (original draft): M. M., H. S. T., I. A., L. J.; writing (review & editing): all authors.

Conflicts of interest

The authors have a patent related to the content of this paper.

Acknowledgements

This work was supported by the ANR (France BioImaging – ANR-10-INBS-04, Morphoscope2 – ANR-11-EQPX-0029, IPGG – ANR-10-IDEX-0001-02 PSL, ANR-10-LABX-31, and ANR-19-CE11-0005), the ITMO Cancer of Aviesan within the framework of the 2021–2030 Cancer Control Strategy on funds administered by Inserm, and the EIC Pathfinder Open DREAM (GA number 101046451).

Notes and references

1 D. Cambié, C. Bottecchia, N. J. W. Straathof, V. Hessel and T. Noël, *Chem. Rev.*, 2016, **116**, 10276–10341.
2 D. Ravelli, D. Dondi, M. Fagnoni and A. Albini, *Chem. Soc. Rev.*, 2009, **38**, 1999–2011.
3 G. Miesenböck, *Science*, 2009, **326**, 395–399.
4 K. Deisseroth, *Nat. Methods*, 2011, **8**, 26–29.
5 Z. Feng, W. Zhang, J. Xu, C. Gauron, B. Ducos, S. Vriz, M. Volovitch, L. Jullien, S. Weiss and D. Bensimon, *Rep. Prog. Phys.*, 2013, **76**, 072601.
6 D. L. Coutu and T. Schroeder, *J. Cell Sci.*, 2013, **126**, 3805–3815.
7 A. Su, S. Grist, A. Geldert, A. Gopal and A. Herr, *PLoS One*, 2021, **16**, e024355.
8 A. Bérces, A. Fekete, S. Gáspár, P. Gróf, P. Rettberg, G. Horneck and G. Rontó, *J. Photochem. Photobiol., B*, 1999, **53**, 36–43.
9 J. Longstreth, F. R. de Gruijl, M. L. Kripke, S. Abseck, F. Arnold, H. I. Slaper, G. Velders, Y. Takizawa and J. C. van der Leun, *J. Photochem. Photobiol., B*, 1998, **46**, 20–39.
10 S. Aslam and K. Edgget, Wearable radiation detector, *US Pat.*, US9024271B2, 2015.
11 P. Foller, I. Fritz, C. Olguin, S. Wrobel, C. Le Maitre, E. Kang and S. Tibbits, Sensing of solar ultraviolet radiation by wearable colorimetry, WO2018232387A1, 2018.
12 U. Megerle, R. Lechner, B. König and E. Riedle, *Photochem. Photobiol. Sci.*, 2010, **9**, 1400–1406.
13 D. Grünwald, S. M. Shenoy, S. Burke and R. H. Singer, *Nat. Protoc.*, 2008, **3**, 1809–1814.
14 H. J. Kuhn, S. E. Braslavsky and R. Schmidt, *Pure Appl. Chem.*, 2004, **76**, 2105–2146.
15 M. Reinfelds, V. Hermanns, T. Halbritter, J. Wachtveitl, M. Braun, T. Slanina and A. Heckel, *ChemPhotoChem*, 2019, **3**, 441–449.
16 G. C. R. Ellis-Davies, *Nat. Methods*, 2007, **4**, 619–628.
17 P. Klán, T. Šolomek, C. G. Bochet, A. Blanc, R. Givens, M. Rubina, V. Popik, A. Kostikov and J. Wirz, *Chem. Rev.*, 2013, **113**, 119–191.
18 J. B. Grimm, A. J. Sung, W. R. Legant, P. Hulamm, S. M. Matlosz, E. Betzig and L. D. Lavis, *ACS Chem. Biol.*, 2013, **8**, 1303–1310.
19 V. N. Belov, C. A. Wurm, V. P. Boyarskiy, S. Jakobs and S. W. Hell, *Angew. Chem., Int. Ed.*, 2010, **49**, 3520–3523.
20 A. Loredo, J. Tang, L. Wang, K.-L. Wu, Z. Peng and H. Xiao, *Chem. Sci.*, 2020, **11**, 4410–4415.
21 J. Tang, M. A. Robichaux, K.-L. Wu, J. Pei, N. T. Nguyen, Y. Zhou, T. G. Wensel and H. Xiao, *J. Am. Chem. Soc.*, 2019, **141**, 14699–14706.
22 J. B. Grimm, B. P. English, H. Choi, A. K. Muthusamy, B. P. Mehl, P. Dong, T. A. Brown, J. Lippincott-Schwartz, Z. Liu, T. Lionnet and L. D. Lavis, *Nat. Methods*, 2016, **13**, 985–988.

23 D. Warther, F. Bolze, J. Léonard, S. Gug, A. Specht, D. Puliti, X.-H. Sun, P. Kessler, Y. Lutz, J.-L. Vonesch, B. Winsor, J.-F. Nicoud and M. Goeldner, *J. Am. Chem. Soc.*, 2010, **132**, 2585–2590.
24 F. M. Raymo, *Int. Scholarly Res. Not.*, 2012, DOI: **10.5402/2012/619251**.
25 D. J. Kozlowski, T. Murakami, R. K. Ho and E. S. Weinberg, *Biochem. Cell Biol.*, 1997, **75**, 551–562.
26 J. A. Clanton, I. A. Shestopalov, J. K. Chen and J. T. Gamse, *J. Vis. Exp.*, 2011, **50**, 2672.
27 W. R. Lempert and S. R. Harris, *Meas. Sci. Technol.*, 2000, **11**, 1251–1258.
28 P. Sengupta, S. B. Van Engelenburg and J. Lippincott-Schwartz, *Chem. Rev.*, 2014, **114**, 3189–3202.
29 M. Fernández-Suárez and A. Y. Ting, *Nat. Rev. Mol. Cell Biol.*, 2008, **9**, 929–943.
30 R. Jasuja, J. Keyoung, G. P. Reid, D. R. Trentham and S. Khan, *Biophys. J.*, 1999, **76**, 1706–1719.
31 F. F. Trigo, J. E. Corrie and D. Ogden, *J. Neurosci. Methods*, 2009, **180**, 9–21.
32 N. I. Kiskin, R. Chillingworth, J. A. McCray, D. Piston and D. Ogden, *Eur. Biophys. J.*, 2002, **30**, 588–604.
33 Y. Zhao, Q. Zheng, K. Dakin, K. Xu, M. L. Martinez and W.-H. Li, *J. Am. Chem. Soc.*, 2004, **126**, 4653–4663.
34 L. Lilge, T. J. Flotte, I. E. Kochevar, S. L. Jacques and F. Hillenkamp, *Photochem. Photobiol.*, 1993, **58**, 37–44.
35 S. R. Bobe, A. M. Raynor, S. V. Bhosale and S. V. Bhosale, *Aust. J. Chem.*, 2013, **67**, 615–619.
36 B. L. Bloodgood and B. L. Sabatini, *Science*, 2005, **310**, 866–869.
37 O. S. Wolfbeis, E. Fürlinger, H. Kroneis and H. Marsoner, *Fresenius' Z. Anal. Chem.*, 1983, **314**, 119–124.
38 B. Finkler, C. Spies, M. Vester, F. Walte, K. Omlor, I. Riemann, M. Zimmer, F. Stracke, M. Gerhards and G. Jung, *Photochem. Photobiol. Sci.*, 2014, **13**, 548–562.
39 R. P. Haugland and K. R. Gee, Photocleavable derivatives of hydroxypyrenesulfonic acids, *US Pat.*, US5514710A, 1996.
40 I. Aujard, C. Benbrahim, M. Gouget, O. Ruel, J. B. Baudin, P. Neveu and L. Jullien, *Chem.–Eur. J.*, 2006, **12**, 6865–6879.
41 D. K. Sinha, P. Neveu, N. Gagey, I. Aujard, C. Benbrahim-Bouzidi, T. Le Saux, C. Rampon, C. Gauron, B. Goetz and S. Dubruille, *ChemBioChem*, 2010, **11**, 653–663.